

THE IRON CALORIMETER AND MUON IDENTIFIER FOR SLD*

A. C. BENVENUTI

INFN Sezione di Bologna, I-40126 Bologna, Italy

G. CALLEGARI, L. PIEMONTESE

*INFN Sezione di Ferrara & Universita di Ferrara, I-44100 Ferrara, Italy*A. CALCATERRA, R. DE SANGRO, P. DE SIMONE, I. PERUZZI, M. PICCOLO
*Lab. Nazionali di Frascati dell'INFN, I-00044 Frascati (Roma), Italy*W. BUSZA, S. L. CARTWRIGHT, J. I. FRIEDMAN, S. FUESS, S. GONZALEZ,
T. HANSL-KOZANECKA, H. W. KENDALL, T. LYONS, L. S. OSBORNE, L. ROSENSON,
U. SCHNEEKLOTH, F. E. TAYLOR, R. VERDIER, D. WILLIAMS, J. M. YAMARTINO
*Massachusetts Institute of Technology, Cambridge, MA 02139*N. BACCHETTA, D. BISELLO, A. CASTRO, M. LORETI, L. PESCARA,
D. TONIOLO, J. WYSS*INFN Sezione di Padova & Universita di Padova, I-35100 Padova, Italy*B. ALPAT, C. ARTEMI, R. BATTISTON, G. M. BILEI, C. CAPPELLETTI,
R. DELL'ORSO, G. MANTOVANI, M. PAULUZZI, M. SCARLATELLA, L. SERVOLI
INFN Sezione di Perugia & Universita di Perugia, I-06100 Perugia, Italy

F. BECONCINI, R. CASTALDI, C. VANNINI, P. G. VERDINI

INFN Sezione di Pisa & Universita di Pisa, I-56010 San Piero a Grado, Italy

B. L. BYERS, D. KHARAKH, R. L. MESSNER, R. W. ZDARKO

Stanford Linear Accelerator Center, Stanford University, Stanford, CA 94309

J. R. JOHNSON

*University of Wisconsin, Madison, WI 53706***Abstract**

The iron flux-return structure for the SLC Large Detector (SLD) has been instrumented with plastic streamer tubes covering an area of about 4500 square meters, to provide muon identification plus energy measurement of hadron showers. A description is given of the production techniques used to construct this large detector system, with an emphasis on the methods by which high reliability and a small number of defects in the completed assembly were ensured.

Submitted to *Nuclear Instruments and Methods*

*Work supported in part by Department of Energy contracts DE-AC02-76ER03069 (MIT), DE-AC03-76SF00515 (SLAC) and DE-AC02-76ER00881 (UW), and by the Istituto Nazionale di Fisica Nucleare.

1. Introduction

The calorimeter system for SLD [1] is designed to provide, with good resolution, measurements of spatial coordinates and energy deposition of electromagnetic and hadronic showers over a wide range of energies (100 MeV to 50 GeV). To achieve this goal, the calorimeter is divided into two main parts:

- (1) inside the solenoid magnet coil, a lead/liquid-argon device with fine sampling to a depth of 22 radiation lengths for electromagnetic showers, followed by coarser sampling to a total depth of about three hadronic interaction lengths; and
- (2) outside the coil, an iron/streamer-tube sandwich with a depth of more than four interaction lengths, which also provides the magnetic flux return.

The liquid-argon calorimeter (LAC) absorbs on the average about 85% of the energy of hadronic events at SLC energies, thus minimizing the degradation of resolution due to unsampled shower energy absorbed in the aluminum coil. The iron calorimeter measures the remaining energy and identifies any muons penetrating the system. The LAC is described in more detail elsewhere [1]. The design and construction of the iron calorimeter are the subject of this paper.

Figure 1 shows an isometric view of the SLD iron structure, which is constructed in the form of an octagonal barrel with planar endcaps. Each octant of the barrel is divided into two sections in depth due to limitations in crane capacity during assembly. The sections are mounted separately on the steel support structures ("arches") and are offset in azimuth to eliminate radial dead zones. Each endcap is similarly subdivided, with the inner section in depth divided in three pieces horizontally, while the outer section is divided in two vertically, again eliminating radial dead regions. The solid angle coverage is complete except for holes in the endcaps to accommodate beamline components, a loss of less than 1%.

Figure 2 shows one quadrant of a cross section of SLD in a plane containing the beam line. Each barrel octant and endcap of the iron calorimeter consists of 14 iron plates 5 cm thick, interleaved with sampling chambers incorporating external readout electrodes with plastic streamer tubes developed by Iarocci and collaborators [2]. Details of the construction of these chambers are provided in the following sections. This technique is

well-matched to large calorimeter systems for several reasons: low materials cost, straightforward mass production, and simple readout electronics, with a high degree of granularity and readout flexibility.

For SLD, the design of the iron calorimeter readout geometry is matched to the two main functions of the device. To act as an extension (or "tail-catcher") of the LAC, its signals must be collected in projective towers that match that system, as shown by the dashed lines in Fig. 2. For optimum identification and tracking of muons in the presence of hadron showers, it is desirable to have a readout with fine granularity. Both goals are achieved, by providing separate electrode sheets on opposite surfaces of each layer of plastic streamer tubes. In most cases, one sheet is simply composed of long narrow strips parallel to and matching in width the individual tubes (1 cm pitch). This gives a granularity equivalent to reading out the anode wires one by one, without the added complication of a large number of high-voltage capacitors. Signals on these strips are recorded simply as digital hits by a low-cost discriminator/shift-register system [3]. The opposing electrode sheet is an array of quadrilateral pads with typical dimensions of 20 to 30 cm on a side, calculated by projecting tower-defining values of polar and azimuthal angles onto the plane of the chamber. Examples of the pad geometry are shown in Fig. 3 (barrel) and Fig. 4 (endcaps). Corresponding pads in successive layers are ganged to form projective towers, and the collected signals are recorded through analog amplifiers and digitized.

Figure 5 shows schematically the chamber arrangement in a typical barrel octant. Note that following the seventh and fourteenth iron plates are double layers of chambers including strips transverse to the tube direction, to provide fully constrained space points for improved muon tracking and rejection of backgrounds from hadron showers and decay.

2. The Modules

2.1 CONSTRUCTION

The plastic streamer tubes were constructed in groups of eight cells, with each group assembled as a separate gas-tight package called a module. Approximately 10,000 such modules were built, ranging in length from 1.9 to 8.6 m. Most of the parts required to make up a module [4] were extruded or molded from PVC or other inexpensive plastic.

These include:

- (1) an extruded profile consisting of eight parallel channels, each 9 mm wide by 9 mm deep and separated by 1 mm thick walls on a 1 mm thick bottom;
- (2) molded end-pieces which attach to the profile and support a small printed circuit board for the wire connections;
- (3) molded bridges which support the wire in the center of each channel;
- (4) molded bridge covers which retain the wires in the bridges;
- (5) an extruded hollow envelope with 1 mm thick walls and inner dimensions 1 cm by 8.15 cm; and
- (6) molded endplugs with gas and electrical feedthrough connections.

A cut-away view of one end of a module is shown in Fig. 6. The circuit boards connect each of the eight wires to a high-voltage bus through a 220Ω resistor. The wire is silver-lubricated beryllium-copper $100 \mu\text{m}$ in diameter.

The channels in the extruded profile must be coated with a conducting layer of sufficiently low resistivity to maintain the DC electric field around the anode wires and to prevent discharges due to surface effects. At the same time, the resistivity must be large enough that nearly the full discharge from passage of a particle can be induced on the external electrodes. In practice, this requires a surface resistivity in the range from about 0.05 to $2.0 \text{ M}\Omega/\text{square}$. Considerable care is required, as the coating must be very thin and uniform to meet the requirements outlined above.

The SLD modules were coated with a mixture of one part of a graphite colloid [4] with eight parts of isobutyl-methyl-ketone, an organic solvent which dissolves PVC and ensures the embedding of the graphite in the surface of the plastic. The long-term stability of this coating has been demonstrated in other experiments using this technique [2]. The mixture was applied [4] with a painting head made of three synthetic sponges saturated with the coating compound. The extrusions were passed under the painting head by a friction transport mechanism. The coating thickness was adjusted by varying three parameters in the operation: the speed of the extrusions past the painting head, the flow of the graphite mixture into the sponges, and the vertical position of the sponges with respect to

the extrusions. After painting, the profiles were passed to a heating station to accelerate the drying of the coating.

Painted extrusions were then checked for correct surface resistivity using a probe with multiple graphite tips. The resistivity in each of the eight channels was measured, and the profile was accepted if all readings were within the range 0.20 to 2.0 M Ω /square. To check the variation with time of the resistivity, as the solvent evaporates from the coating, one of every twelve extrusions was set aside and rechecked regularly over the following three days. The typical variation observed was about a factor of two reduction in resistivity, and no significant further change was found after the three-day period. Extrusions with initial resistivity values between about 2 and 5 M Ω /square were rubbed with felt pads to reduce the resistivity to the acceptable range. The distribution of resistivities measured on 2000 finished profiles is shown in Fig. 7. The mean value of the resistivity is about 0.5 M Ω /square. Including the rejection of profiles due to flaws in manufacture, the rejection rate at this stage was about 25%. As a further quality control check, about 5% of the extrusions from each coating run were set aside, wired and assembled into modules, and tested with gas and high voltage as described below for the final production stage.

The first step of the final module assembly procedure was to cut profiles and envelopes to length. The tops of the profile channel walls were then given an additional heavy coating of graphite paint using a felt pad, and one end was painted with a brush to provide a conductive path to a piece of copper tape under the profile (to be used for a ground connection). The graphite paint used for this step was the same as described above. The extra coating was found to be important, as it substantially reduces the incidence of discharges from the tops of the channel walls.

Molded end-pieces with circuit boards were then attached to the profiles, and bridges were installed approximately every 35 cm along the extrusion. Next, all eight wires of a module were strung in one pass, with a nominal tension of 250 g maintained by a constant drag mechanism. After soldering the wires to the circuit boards at each end, the tension was checked mechanically and bridge covers were installed, followed by a visual inspection. The wired profile was then inserted into a matching extruded envelope. During insertion, the profile passed under a vacuum cleaning head and an automatic device which checked for laterally misplaced wires. At one end, a ground wire was soldered to the piece of copper

tape mentioned above, and a high-voltage lead was soldered to the bus of the circuit board at that end. These wires were then soldered to the appropriate electrical feedthrough connections on a molded endplug, and this plug (together with another at the far end) was sealed into the envelope with a PVC solvent cement.

The completed modules were checked for gas leaks by immersion in a tank of water while maintained at a gauge pressure of 50 millibar. Finally, the modules were later checked for proper electrical connections by measuring the capacitance between the high voltage and ground feedthroughs on the appropriate endplug, using an impedance bridge operating at low frequency (12 Hz) to minimize effects of the variation of resistivity in the graphite coatings. With this technique, modules with all connections intact were found to have a capacitance of about 100 pF per meter of length, while any open connections would cause a substantially lower reading.

2.2 HIGH-VOLTAGE TESTING

One important requirement of the modules is a high degree of reliability in operation, given the very large number of units and the inaccessibility of much of the system. Accordingly it was desirable to perform tests capable of identifying cases which had a higher than normal probability of failure during the course of the experiment. Here failure of a module means that at operating voltage it draws a continuous anode current large enough to cause a serious degradation in performance (more than about 10 μA in practice). Experience with these modules [5] indicates that there is a strong correlation between eventual failure and earlier abnormal behavior of the anode current, e.g., higher than normal values either continuously or in bursts. Thus it was decided to subject each module to a series of high-voltage tests covering several days, during which the anode current would be monitored, and to apply a stringent set of acceptance criteria based on the results.

Figure 8 shows a diagram of the circuit used for the tests. Depending on the test phase, the high voltage was provided either by a computer-controlled multichannel system [6] with current readout for each channel (preacceptance phase), or by a set of dual NIM modules [7] with an overcurrent trip feature and computer-monitored current output

(final acceptance test). For the final phase, currents drawn by individual modules were monitored by recording the voltage drop on resistors in the ground return connections, using a multichannel low-voltage monitoring system [8]. The modules were filled with a gas mixture of three parts isobutane to one part argon. The gas was mixed continuously from bulk storage of the components, using electronic mass-flow controllers [9]. The bulk isobutane had a typical analysis of roughly 99% isobutane with the balance primarily normal butane and propane. Normally the gas flowed through parallel chains of 40 modules in series, with each chain receiving a flow of about 0.12 L/min during the tests, corresponding to one complete volume change in about 24 hours. The system was purged at a higher rate, with up to ten volume changes prior to the tests.

2.2.1 Preacceptance tests

The preacceptance step was intended to weed out obviously bad modules prior to the more detailed acceptance test. The first phase was called conditioning, and consisted of a programmed increase in the high voltage applied to a group of modules. The voltage was first set at 4.0 kV for three minutes, then turned off for two minutes, then raised to 4.1 kV for three minutes, then off again, and so forth until 4.9 kV was reached without excessive current being drawn. Each computer-controlled high-voltage channel was connected to ten modules in parallel, as shown in Fig. 8. If at any voltage step the current drawn from any channel exceeded 20 μA , the voltage of that channel was turned off, then returned to the preceding step for another attempt. This was allowed to continue for up to 72 hours. After reaching 4.9 kV successfully, the voltage of a channel was reduced to 4.8 kV and maintained for the balance of the 72 hour period. Any module failing to reach 4.9 kV, or drawing over 5 μA for more than one hour at 4.8 kV, was isolated, disconnected, and declared a failure.

The second phase of the preacceptance tests consisted of maintaining a constant voltage of 4.8 kV for a period of six days, during which the currents drawn by groups of ten modules were checked every 12 hours. If a group were found to be drawing more than 20 μA , the individual module(s) responsible for the excess current would be isolated and disconnected as a failure.

2.2.2 Final acceptance test

The final test phase consisted of maintaining a constant voltage of 4.8 kV for an additional 72 hours, with no current monitoring for the first 24 hours but with continuous monitoring of currents drawn by individual modules during the last 48 hours. These data allowed detailed study of the behavior of the modules. Figure 9 shows the distribution of individual average currents drawn during the 48 hours, for about 3000 modules. Based on this distribution, any module averaging more than $0.1 \mu\text{A}$ for this period was declared a failure. A high average current could be the result of steady current or of one or more excursions to higher values. Figure 10 shows a histogram of the maximum current drawn by each module during the 48-hour period. In most cases, the maximum current was achieved for only a few seconds, and longer excursions represented abnormal behavior. A module found to have exceeded $1.0 \mu\text{A}$ for any period of greater than one minute was declared a failure. As expected, the two criteria are somewhat correlated. Figure 11 shows the distribution of average currents for modules failing the second criterion, and it is clear that a much higher proportion of these fail the first criterion in comparison with Fig. 9.

2.2.3 Results

Data from the preacceptance tests were recorded by the IBM PC-XT computer controlling and monitoring the multichannel high voltage system. For the final acceptance test, the low-voltage monitoring system recording the individual module currents was operated by a VAX 11/780 computer which logged the results on magnetic disk. After analysis of the data, failures were marked clearly on the modules themselves, recorded on printed lists according to module serial number, and entered in a database using the NOMAD2 management code on the SLAC main computer system. The module serial numbers, which are also marked on the modules themselves using printed labels, contain dates and batch numbers for extrusion coating and for module assembly. Thus the database allows studies of the correlation of failures with module history. A summary of failure rates as a function of acceptance-test batch number (each batch was about 200 modules tested simultaneously) is given in Table I for the modules constructed for the barrel section. The total rejection fraction includes failures due to leaks or disconnected wires inside the module. The overall rejection rates are comparable with those experienced

by other large-scale experiments using plastic streamer tubes of similar construction [10]. A long duration test [5] performed on 1600 modules indicates that modules passing all the acceptance criteria will fail in actual operation at a rate less than 2% per year at 90% confidence level, assuming the failure rate is independent of time.

3. The Chambers

3.1 CONSTRUCTION

The term "chamber" is used here to mean a complete detector unit including several (from three to 22) modules side-by-side, with appropriate electrode sheets (longitudinal strips, transverse strips, or pads) attached to opposite surfaces, as described briefly in the introduction. The lengths and widths of the various chambers for SLD were chosen to satisfy certain design constraints:

- (a) dimensions of the available spaces in the iron structure;
- (b) dimensions of available material for electrode sheets;
- (c) relative ease of installation or possible later removal; and
- (d) in the barrel, alignment of chamber edges with pad (tower) row boundaries.

The strip electrode sheets were made from a layer of 1.6 mm thick fiberglass [11] with 0.040 mm thick copper foil bonded to both surfaces. Since this material was extruded continuously rather than laminated in a press, the sheets were cut to the full length of each chamber (up to 8.6 m) with a maximum width of 1.2 m. Figure 12 shows a sample of the strip electrode pattern for chambers in the barrel section. The pattern was created on one surface by milling away 1 mm wide paths in the copper foil along parallel lines running the full length of the chamber (longitudinal strips) or across the width of the chamber (transverse strips). The milling head was moved by a computer-controlled routing machine [12] while the sheet was held stationary. The longitudinal strips were cut to match the module wires, on a 1 cm pitch but with additional space at the edges of each group of eight. The transverse strips were cut on a 2 cm (endcaps) or 4 cm pitch (barrel). In addition, for the barrel the longitudinal strips were modified at one end as shown in Fig. 12, to form card-edge connectors with eight traces on a 2.54 mm pitch. The traces were later gold-plated. This allowed for connection to electronics using mass-termination connectors on

flat multiconductor cable. For transverse strips and endcap longitudinal strips, the wires in the flat cable were soldered directly to the copper foil, due to constraints of geometry. In all cases, the copper foil on the opposite surface of the fiberglass served as a ground sheet. Wires in the flat cable which connected to strips alternated with wires connected to this ground sheet.

The pad electrode sheets were made from 0.8 mm thick fiberglass with 0.04 mm thick copper foil laminated on one side [11]. The electrode patterns were created using the same milling/routing machinery described above. Since the patterns (Figs. 3 and 4) are in general symmetric about the midline of a chamber, it was convenient to cover only one-half the length of a chamber with a single sheet. Appropriate wiring was used to bring connections to the pads out to each end of each chamber, where they could be ganged into towers later. For the barrel, the pads lie in straight rows, so the wiring was performed conveniently by soldering to the pads appropriate wires in flat multiconductor cable with mass-termination connectors at the ends of the chamber, as shown in Fig. 13(a). For the endcaps the geometry is more complex, so the connections were made by soldering short jumper wires from the pads to traces on a long, narrow strip of copper-clad fiberglass with a multipin connector soldered to the end, as shown in Fig. 13(b). The traces were created mechanically with a set of ganged circular saw blades in place of a milling head. In both cases the pads and wiring were covered with an insulated sheet of metal foil to provide a ground plane. For the barrel, this sheet was 0.05 mm thick aluminum with 0.4 mm thick PVC laminated to both sides, while for the endcaps the material was 0.04 mm thick copper laminated to 0.5 mm thick fiberglass on one side.

The chambers were assembled using a high-strength pressure-sensitive transfer adhesive [13] to fasten together the different layers of a chamber package. After first cleaning the surface, adhesive was applied over the strip pattern on a strip electrode sheet. For the barrel, modules of a matching length were then selected, cleaned and set on the exposed adhesive aligned with the strip pattern, with 0.75 mm thick strips of paper inserted between the modules as required to maintain tight contact. After application of another layer of adhesive to the exposed surface of the modules, matching pad sheets were set in place with the pad pattern and accompanying wiring facing up, away from the modules. Strips of plastic filler material (1 mm-thick styrene for the barrel) were then placed between

the wiring and attached to the pad pattern with more adhesive. After another layer of adhesive was applied to the exposed surface of the filler material, a matching insulated ground sheet was installed as the final layer of the basic chamber. The pad ground sheet was then connected to the strip ground plane using short jumper wires, and the modules within the chamber were interconnected in series for gas flow using short lengths of plastic tubing. Finally, the completed unit was covered with a flexible membrane, and the space between the membrane and the flat assembly table was evacuated for 30 minutes, to ensure good bonding of the adhesive and flatness of the finished chamber.

Assembly of the chambers for the endcaps was performed in a similar manner, but the modules were not attached directly to the electrode sheets. In place of each module a hollow extruded plastic sleeve was installed, with a rectangular cross section of inner dimensions slightly larger than the outer dimensions of a module. After the rest of the chamber package was completed, the modules were inserted into these sleeves and interconnected for gas flow. Although this technique creates slightly more inactive area in a chamber, it provides certain advantages: the modules are more easily replaced in case of damage or later failure; chamber packages may be transported long distances with no risk of damage to the modules; and module assembly and testing may proceed in a different place and on a schedule not directly linked to chamber lamination.

3.2 QUALITY CONTROL AND TESTING

Besides the high voltage testing of modules described above, all critical parts of a chamber were checked carefully for quality at each step of manufacture and assembly. In addition, every completed chamber was tested with cosmic rays under operating conditions of gas and high voltage to ensure the correct operation of the finished detector.

After each electrode sheet was completed, it was subjected to electrical tests to check for such defects as incorrect wiring pattern, open connections, short circuits between electrodes, or short circuits to ground. A signal (DC, AC or pulse) was injected on each electrode in turn, and a sensing circuit indicated the appearance (or absence) of the signal at the corresponding trace or pin of the appropriate connector. Defects then were corrected immediately. At the stage of chamber assembly, the electrodes were checked again by measuring in turn the capacitance of each electrode to ground, using a commercial hand-held

meter. As this measurement can be made quickly and conveniently without access to the electrodes themselves, it was repeated after chamber assembly and again after installation. Short circuits detected at this stage were normally corrected by connecting a low-voltage high-current power supply across the shorted elements to burn out the connection, usually caused by a small filament of copper left by the milling operation. Such a connection was often sensitive to pressure on the electrode sheets, and thus may not have been present at the time of an earlier test. Finally, the modules in a completed chamber were checked again for correct capacitance of the sense wires to ground, and the chamber as a whole was pressurized to a gauge pressure of 7.5 mbar and checked for leaks. A module found to have a broken wire or a nonrepairable leak was replaced.

Tests of each completed chamber with cosmic rays were performed at a high voltage of 4.65 kV with the same gas mixture as for the module tests (three parts isobutane to one part argon). Data were taken using a multichannel data acquisition system (about 1000 channels). Figure 14 shows a diagram of this system. The cosmic ray trigger was provided by a coincidence of large scintillation counters (1.5 m square) placed above and below the chambers to be tested. The charge induced on individual pads and strips was integrated by an array of low-noise amplifiers [14] and stored on a multiplexed system of sample-and-hold modules [15]. Digitization was performed by a microprocessor-based ADC module [16] which then subtracted pedestals and stored only values exceeding a programmed threshold. Results were recorded and analyzed by a VAX 11/780 computer.

Figure 15 shows separate pulse-height distributions for the charge induced on the strips (a) and pads (b) of a typical chamber during a run of about 3000 cosmic rays, together with a scatterplot (c) showing the correlation of the two. Since the induced signal may, in general, be spread among more than one electrode, each entry in a histogram was calculated by finding the electrode with the largest pulse height and adding to it the signals from nearest neighbors. The significant scatter between strips and pads seen in the correlation is understood as due to variations in the direction of streamers azimuthally about the wire. Figure 16 shows a scatterplot of the sum of strip plus pad pulse heights against the signal collected on the anode wire. Here the correlation is very good, showing that the total charge induced on the electrode sheets was indeed equal to that deposited on the wire. This charge was measured to be approximately 25 pC.

To detect possible defects such as disconnected anode wires, two quantities were calculated for each electrode within each run: (a) the number of events for which that electrode had the largest signal, and (b) the average signal of that electrode plus nearest neighbors for those events. Figure 17 shows graphs of these quantities versus channel number for the strip electrodes of one chamber in a particular run. An example of a disconnected wire is evident in Fig. 17(a) as a channel with very few "hits" compared with its neighbors. Fewer than 0.1% of the wires in completed chambers were found to be disconnected, apparently not detected by previous capacitance measurements due to intermittent contact on the internal printed circuit boards. After correcting for gain variations in the electronics, average pulse heights were found to vary somewhat over a chamber and from chamber to chamber, with an overall root-mean-square variation of the order of 10%. In addition, the alignment of the strip electrodes with the anode wires was checked by calculating and plotting, for each strip hit, the asymmetry of the signals induced on the neighbors of that strip. In most cases the strip centering and alignment was found to be better than about ± 1 mm over a complete chamber.

The cosmic-ray tests also served as an additional high-voltage check of the modules after handling. Approximately 0.5% of the modules were rejected and replaced at this stage, for a variety of reasons.

4. Summary

The SLD iron calorimeter has been instrumented with layers of sampling chambers based on plastic streamer tubes. Using the techniques and tests described in this paper, the chambers were produced on schedule and with the level of quality required to operate as a successful detector. As installed, the fraction of inoperative detector elements (shorted modules, disconnected anode wires, shorted or disconnected electrodes) was in all cases less than one in a thousand. Measurements in a test beam of high energy particles [17] showed that the completed iron calorimeter will be able to measure hadronic energy deposition with a resolution of approximately $\sigma_E = 0.8 \sqrt{E}$ (E in GeV) and to track muons with a spatial resolution of about $\sigma_x = 3.7$ mm in each layer. Long duration tests of large numbers of modules have shown that streamer tube failure rates in operation should be less than 2% per year, so the device is expected to run successfully for many years.

Acknowledgments

The successful design and construction of this detector system could not have been accomplished without the help of a large number of skilled people. Particular thanks are due to F. Babucci, G. Bonora, U. Cazzola, D. Ross and D. Sawyer for their dedicated efforts and contributions. The authors would also like to acknowledge the able technical assistance of the following: V. Giordano and A. Zucchini (Bologna); S. Bigoni, V. D'Orto, and C. Fordiani (Ferrara); D. Pistoni (Frascati); the Campana crew (MIT); G. Marinolli, B. Migliorato, and A. Paonessa (Padova); E. Babucci and G. Chiocci (Perugia); F. Bosi, L. Corucci, G. Fausto, and L. Zaccarelli (Pisa); and N. Erickson, J. Escalera, M. Mittmann, P. Ritson, and the crews at IR-6 and the Light Assembly Building (SLAC). In addition, we would like to express our appreciation for the extensive use of the routing machinery at the Fermi National Accelerator Laboratory.

This work was supported in part by the Department of Energy (USA) under contract numbers DE-AC02-76ER03069 (MIT), DE-AC03-76SF00515 (SLAC) and DE-AC02-76ER00881 (UW), and by the Istituto Nazionale di Fisica Nucleare (Italy).

References

1. SLD Design Report, SLAC-Report 273 (1984). M. Breidenbach, IEEE Trans. Nucl. Sci. NS-33, 46 (1986).
2. E. Iarocci, Nucl. Instrum. Methods 217, 30 (1983). G. Battistoni *et al.*, Nucl. Instrum. Methods 217, 429 (1983); A245, 277 (1986).
3. F. Beconcini *et al.*, IEEE Trans. Nucl. Sci. NS-35, 311 (1988).
4. The plastic parts were provided by Costruzioni Meccaniche Bindi, San Giustino, Italy. The graphite colloid was DAG 305 supplied by Acheson Colloiden, Scheemda, Holland. The painting apparatus was developed and operated at the Laboratori Nazionali di Frascati, Rome, Italy.
5. A. Benvenuti *et al.* (the SLD Iron Calorimeter collaboration), to be submitted to Nucl. Instrum. Methods.
6. SY127 High Voltage System, CAEN, Viareggio, Italy.
7. Model 1755P, Bertan Associates, Syosset, NY 11791.
8. J. Kieffer, IEEE Trans. Nucl. Sci. NS-28, 646 (1981).
9. Datametrix-Dresser Industries, Wilmington, MA 01887.
10. W. Busza, Nucl. Instrum. Methods A265, 210 (1988).
11. Material for all strip electrode sheets and for endcap pad sheets and ground planes was supplied by Glasteel Industrial Laminates, Duarte, CA. Barrel pad sheets were standard FR4 material manufactured by DITRON srl, Cerano, Italy.
12. Milling/routing machinery for creating the barrel strip and pad patterns was developed and operated at INFN Sezione di Perugia, Perugia, Italy, and at Universita di Ferrara, Ferrara, Italy. Details may be found in: R. Battiston *et al.*, Universita di Perugia preprint, in preparation; and G. Bonora *et al.*, Universita di Ferrara preprint, in preparation. The endcap strip and pad patterns were produced by a machine built by the Gerber Scientific Instrument Co., Hartford, CT which was modified and operated at the Fermi National Accelerator Laboratory, Batavia, IL 60510. For details, see: C. Lindenmeyer, Fermilab-TM-1257, May 1984.

13. 3M Type Y-9485 and Y-926, 3M Company, St. Paul, MN 55144.
14. E. Cisneros *et al.*, IEEE Trans. Nucl. Sci. NS-28, 465 (1981).
15. E. Cisneros *et al.*, IEEE Trans. Nucl. Sci. NS-24, 413 (1977).
16. M. Breidenbach *et al.*, IEEE Trans. Nucl. Sci. NS-25, 706 (1978).
17. G. Callegari *et al.*, IEEE Trans. Nucl. Sci. NS-33, 201 (1986).

Table 1:

Results in percent from tests performed on more than 6000 barrel modules. The first row reports "early" failures (during preacceptance tests), while the second row shows rejection rates during the final acceptance test. The last row gives the total rejection fraction, including failures due to gas leaks or disconnected wires.

Batch Number	901	902	903	904	905	906	907	908	909	910	911
Preacceptance Failures	12.4	8.0	10.0	8.1	4.6	6.3	3.0	2.0	4.0	4.0	8.5
Acceptance Failures	9.4	17.5	6.9	16.9	7.9	15.8	11.5	5.0	4.0	3.0	1.5
Total Rejection	23.5	30.5	22.5	30.0	16.3	27.5	17.5	9.0	15.0	13.5	12.5

Batch Number	912	913	914	915	916	917	918	919	920	921	922
Preacceptance Failures	8.5	9.0	6.5	11.5	5.5	5.5	2.5	10.0	7.0	12.0	6.0
Acceptance Failures	2.0	13.5	16.5	3.5	19.5	13.0	15.0	1.5	7.0	21.0	22.0
Total Rejection	14.5	23.0	25.0	17.5	24.5	21.5	19.5	13.5	15.5	34.0	28.0

Batch Number	923	924	925	926	927	928	929	930	931	932	933
Preacceptance Failures	3.0	5.5	8.5	1.5	7.5	7.0	5.0	2.5	3.5	3.5	4.0
Acceptance Failures	16.5	15.0	13.0	17.0	18.0	12.5	13.0	9.5	6.0	16.9	12.0
Total Rejection	21.0	21.0	22.0	18.5	27.5	21.0	19.0	12.5	11.0	22.5	19.0

Figure Captions

- Fig. 1. Isometric drawing of the SLD iron structure.
- Fig. 2. Cross-section drawing of SLD, one quadrant. Dashed lines indicate boundaries of projective towers in the calorimeter system.
- Fig. 3. Pad geometry of one-half the length of a typical barrel layer. The other half is a mirror image.
- Fig. 4. Layout of pads in one quadrant of a typical endcap layer.
- Fig. 5. Arrangement of chamber layers in a typical barrel octant. The endcap arrangement is similar.
- Fig. 6. Cutaway view of the end of a module with high-voltage and ground connections. The other end is similar, except that the PC board has no resistors or HV bus, and there are no connections to the outside of the module.
- Fig. 7. Distribution of surface resistivities of the graphite coating on approximately 2000 extruded profiles.
- Fig. 8. Circuit diagrams for the high-voltage testing of modules.
- Fig. 9. Distribution of time-averaged currents drawn by approximately 3000 individual modules during the 48-hour final acceptance test.
- Fig. 10. Distribution of maximum currents drawn during the final acceptance test.
- Fig. 11. Average currents drawn by modules which exceeded one microamp for periods greater than one minute.
- Fig. 12. Strip electrode pattern for barrel chambers.

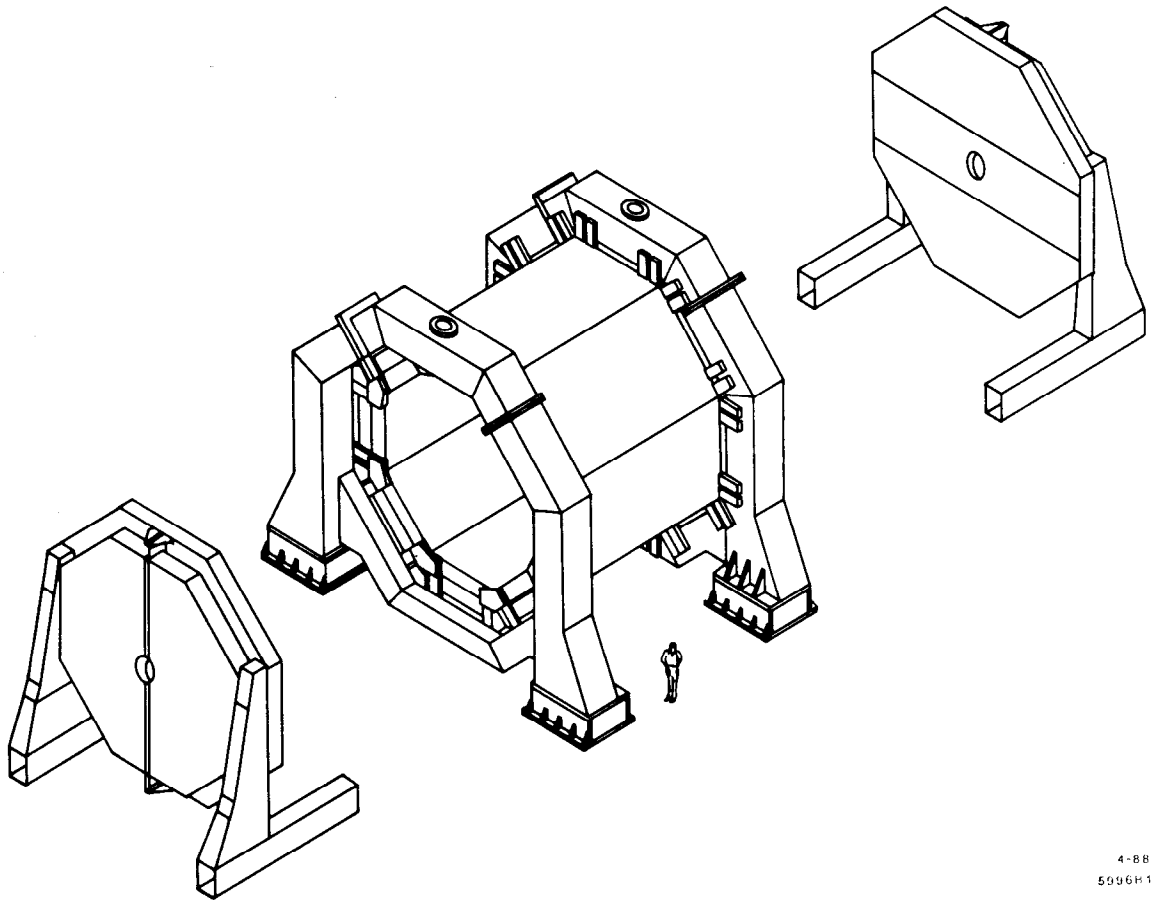
Fig. 13. (a) Wiring of a typical row of pads in one-half of a barrel chamber. Even-numbered wires in a flat multiconductor cable are soldered to the pads in order, while odd-numbered wires are grounded at the end of the chamber. (b) Typical pad wiring on one-half of an endcap chamber. Individual solder connections are made with short pieces of insulated wire between pads and corresponding traces on one surface of a strip of copper-clad fiberglass. The other surface is insulated from the pads and grounded at the end of the chamber.

Fig. 14. Data acquisition system for the cosmic-ray tests of completed chambers.

Fig. 15. (a) Distribution of pulse heights induced on the strip electrode sheet of a typical chamber during a cosmic-ray test. (b) Corresponding distribution for the pad sheet of the same chamber. (c) Scatterplot showing the correlation of individual entries in (a) and (b).

Fig. 16. Scatterplot showing the correlation between signals deposited on the anode wires of a chamber, and the sum of those induced on the pad and strip electrode sheets.

Fig. 17. (a) Histogram versus strip number, of the number of events in a cosmic-ray run for which each strip electrode showed the largest signal. (b) Average signal from each strip (added to that of nearest neighbors to allow for signal sharing) for the events in which that strip showed the largest signal.



4-88
5096P1

Fig. 1

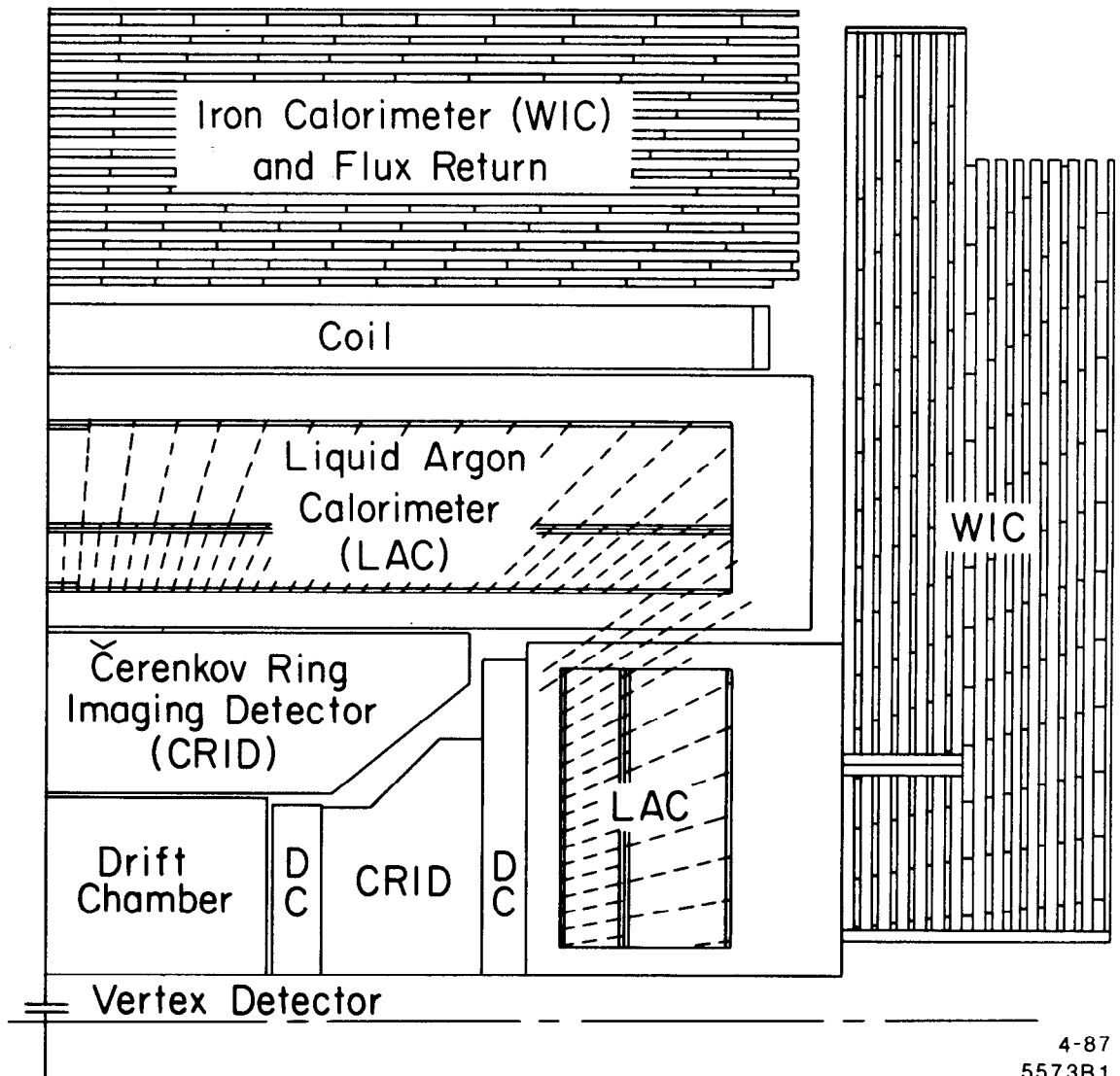
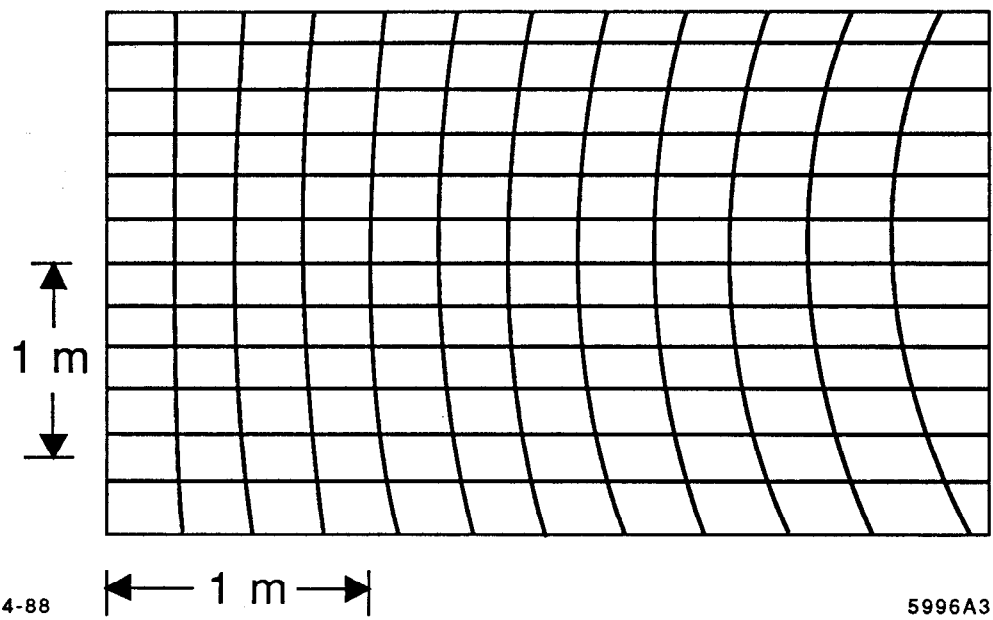


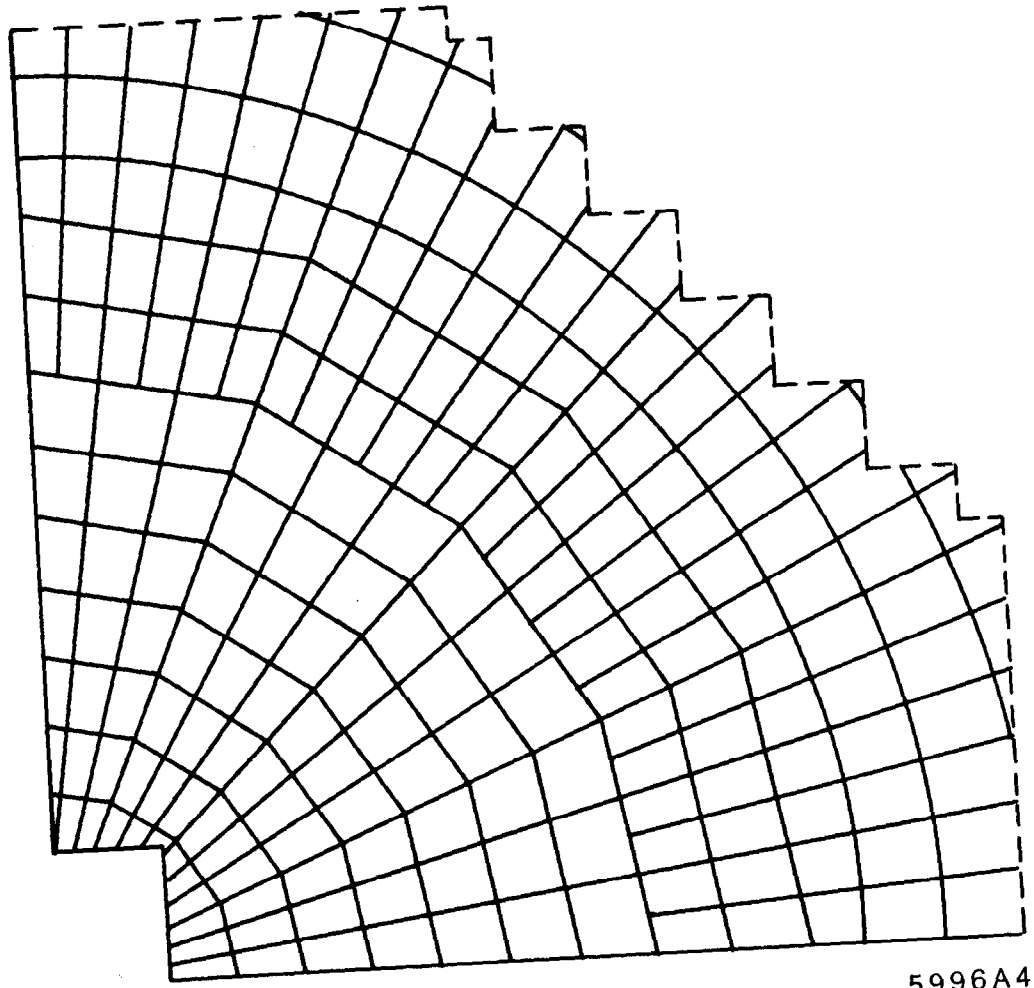
Fig. 2



4-88

5996A3

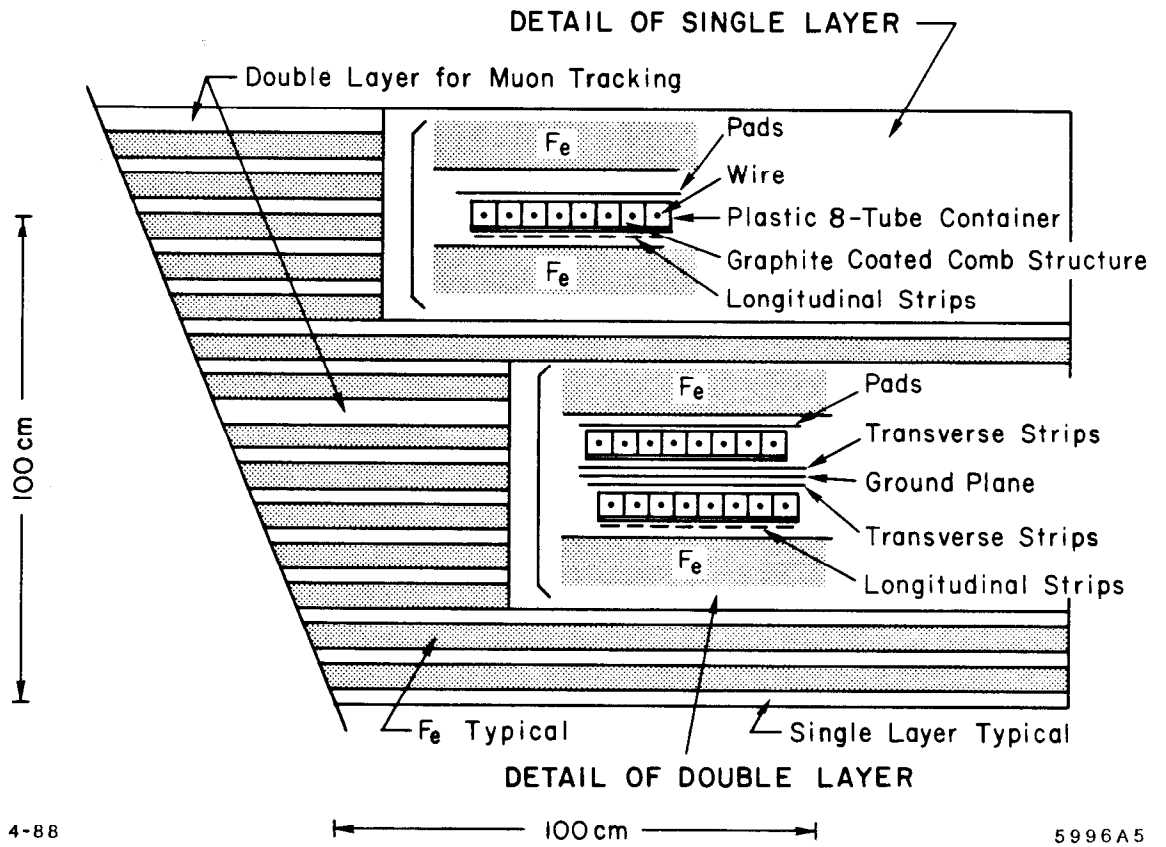
Fig. 3



4-88

5996A4

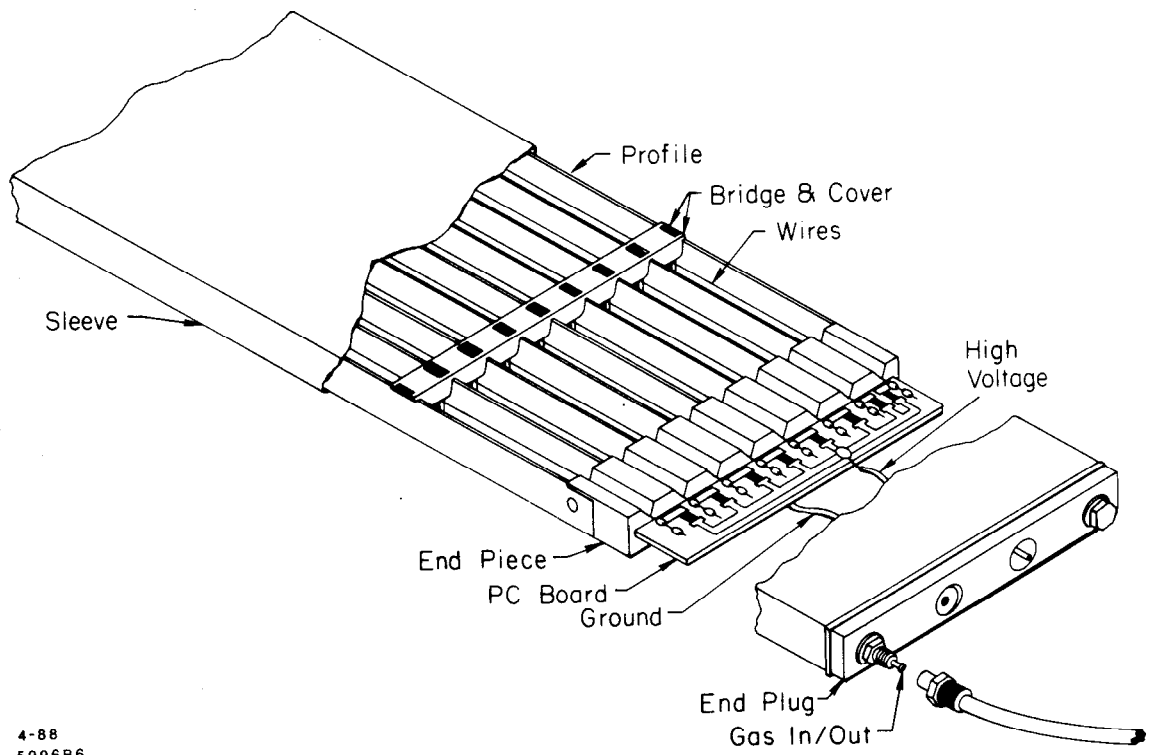
Fig. 4



4-88

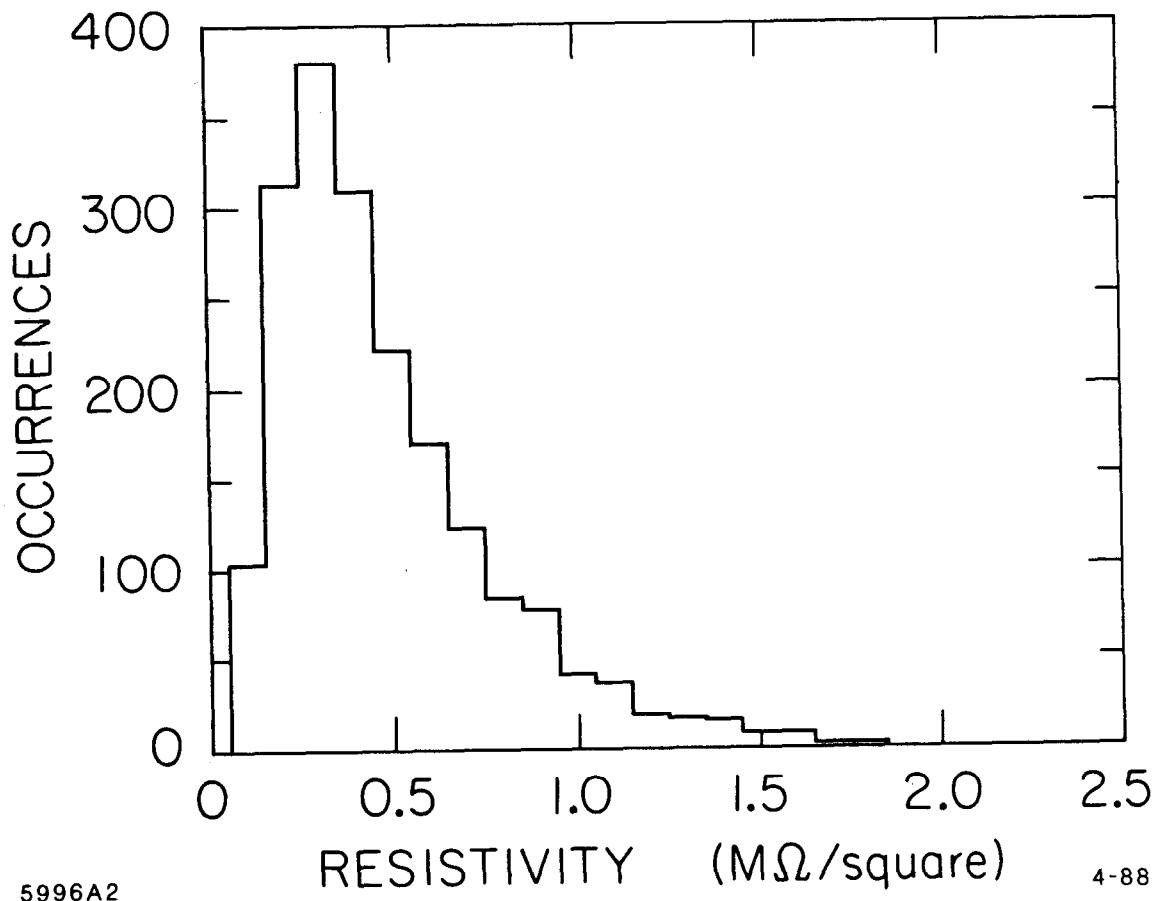
5996A5

Fig. 5



4-88
5996B6

Fig. 6

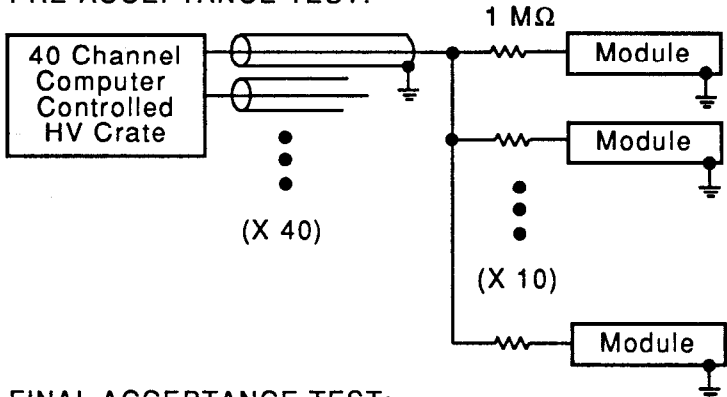


5996A2

4-88

Fig. 7

PRE-ACCEPTANCE TEST:



FINAL ACCEPTANCE TEST:

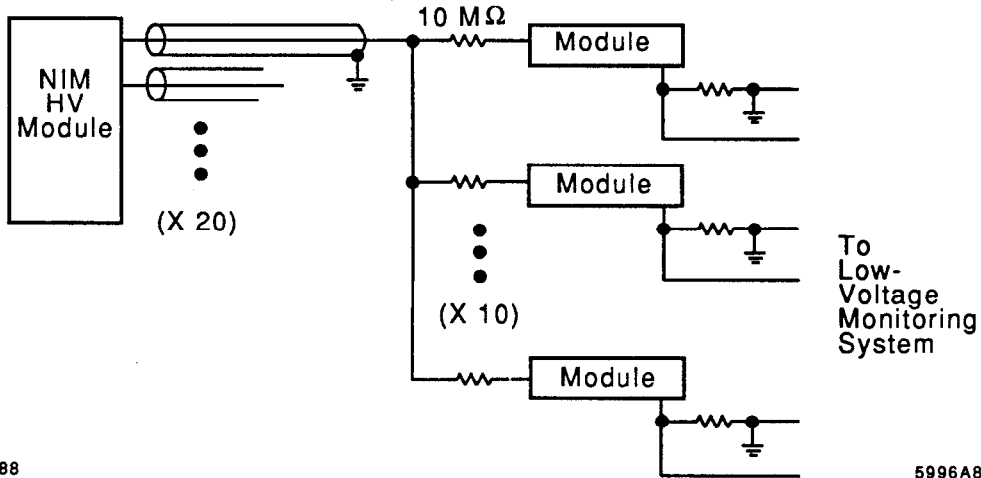
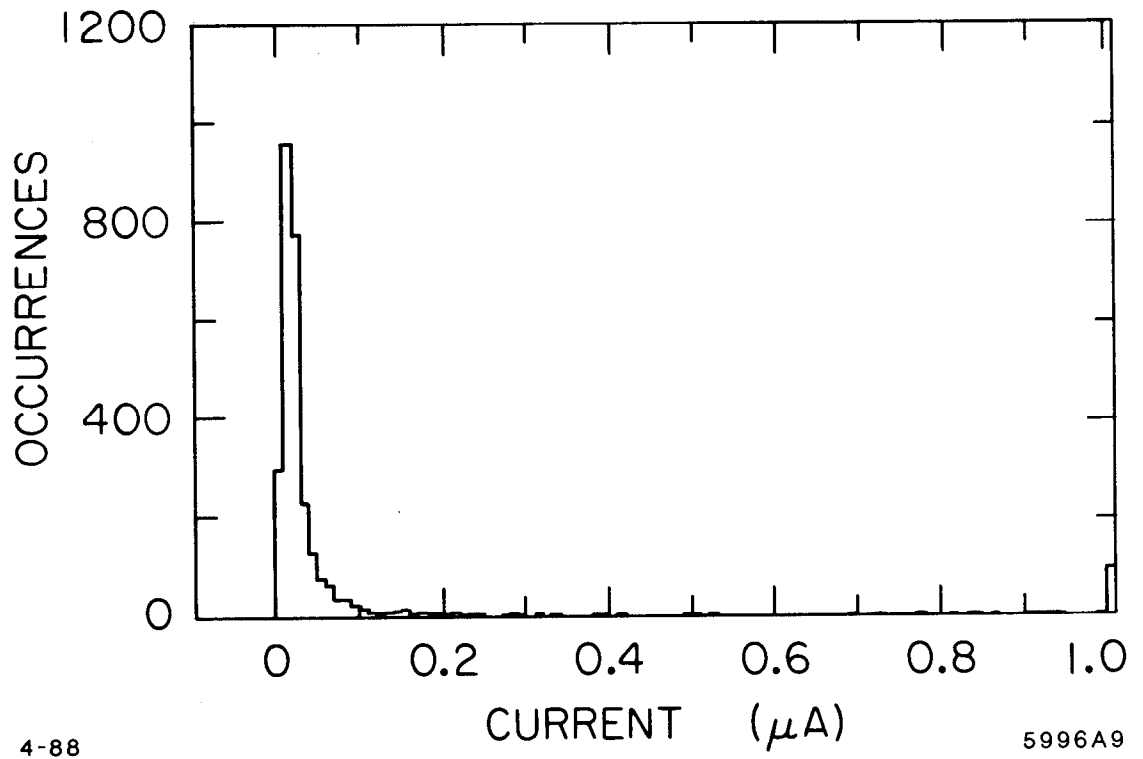


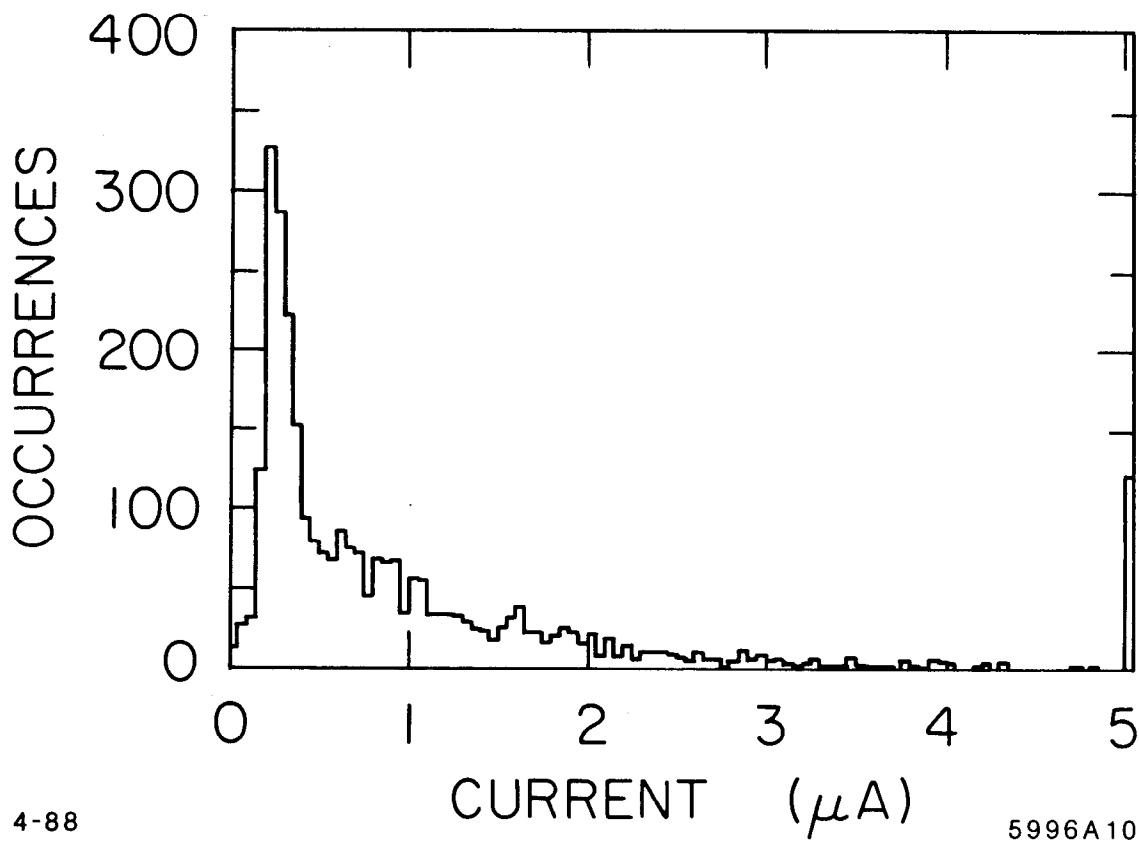
Fig. 8



4-88

5996A9

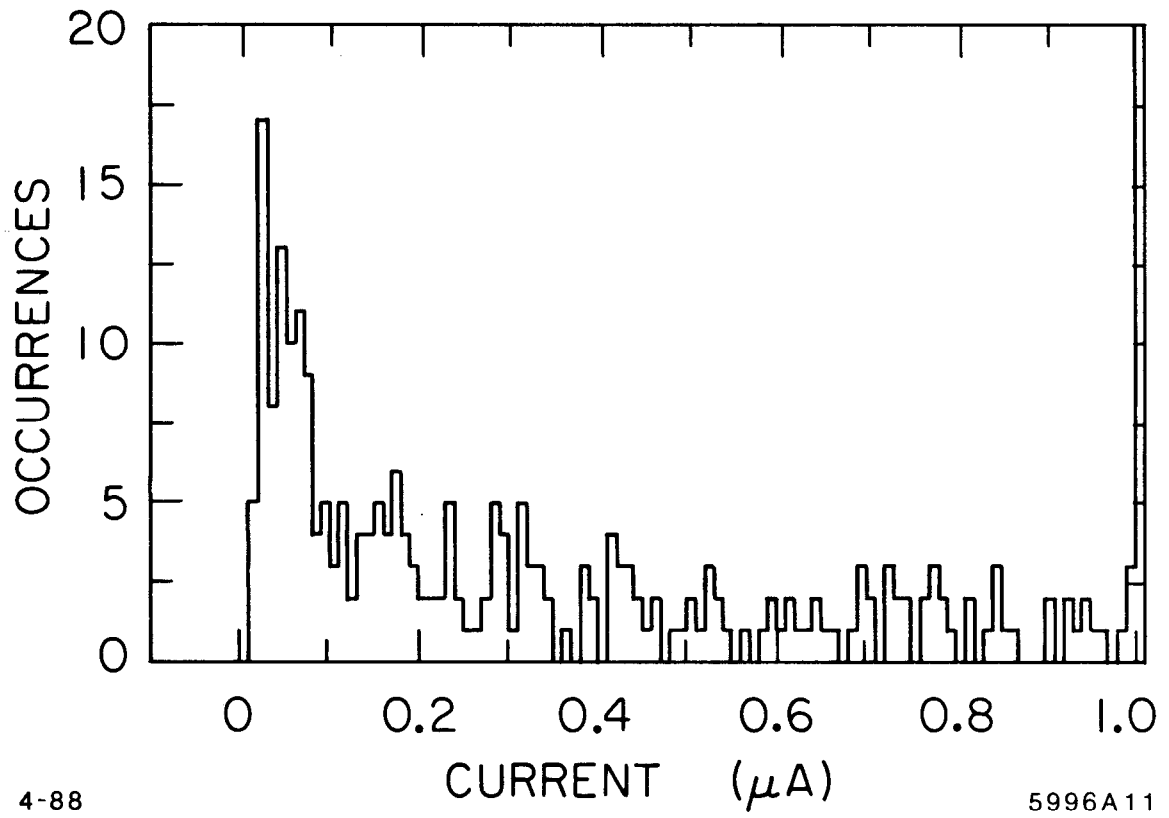
Fig. 9



4-88

5996A10

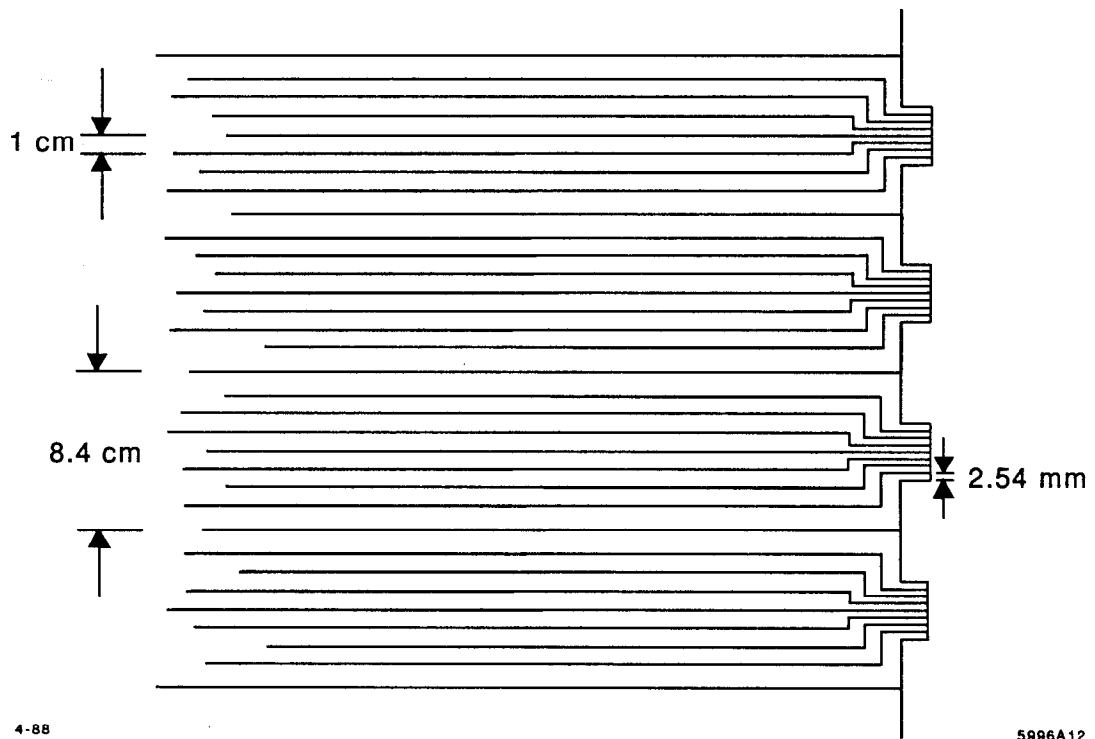
Fig. 10



4-88

5996A11

Fig. 11



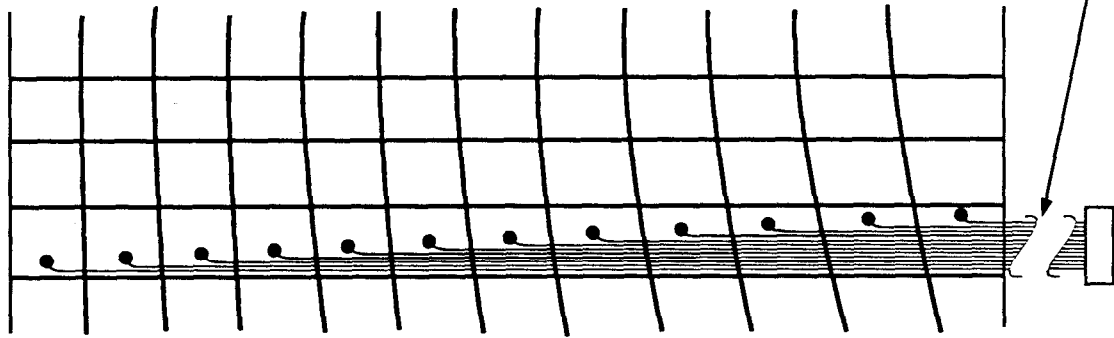
4-88

5996A12

Fig. 12

(a)

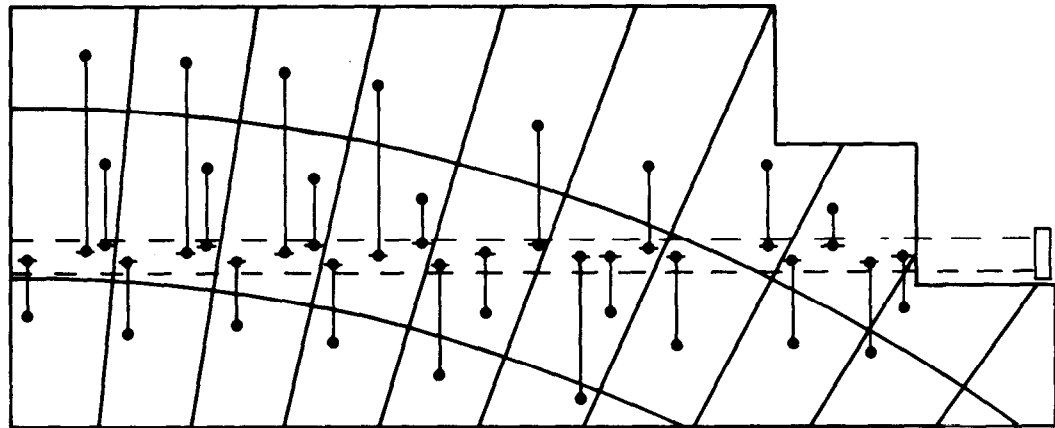
Cable Typical



5-88

5996A13

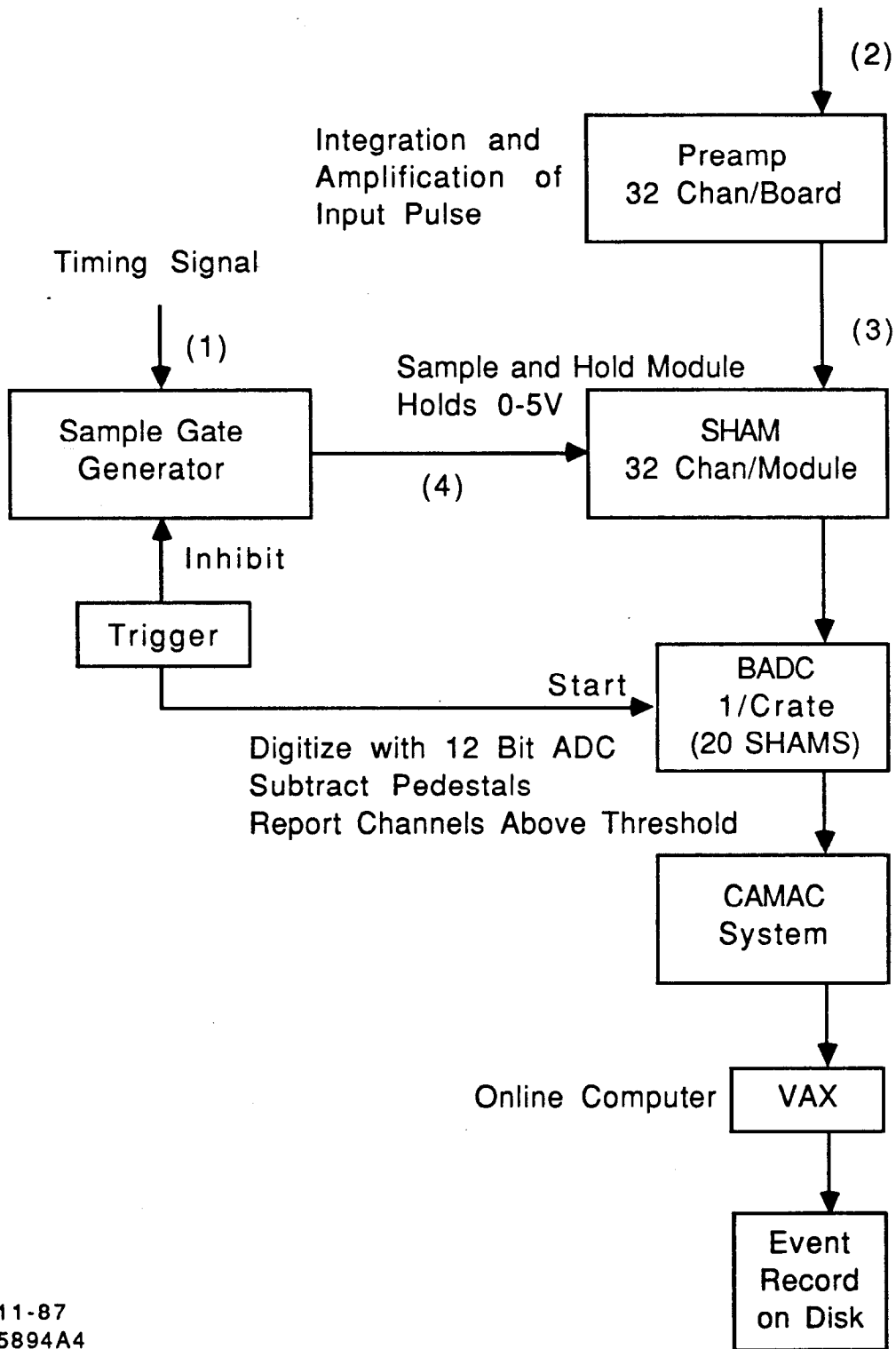
(b)



4-88

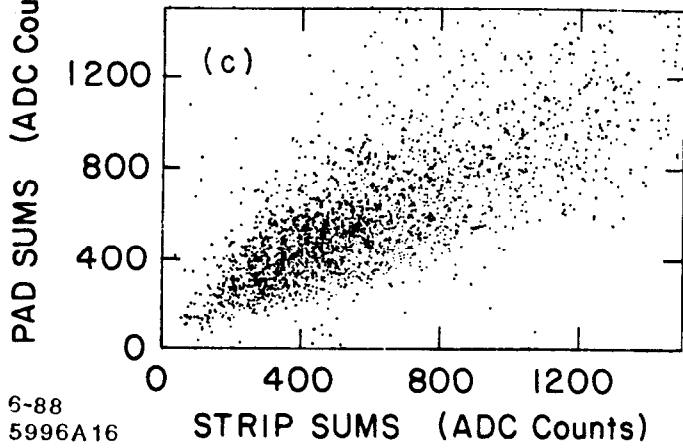
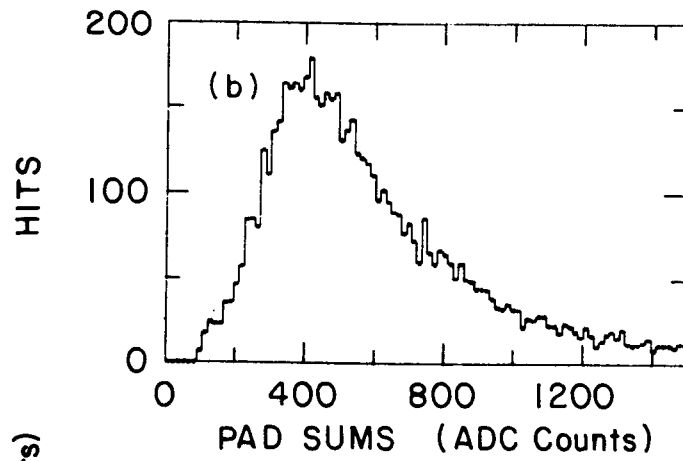
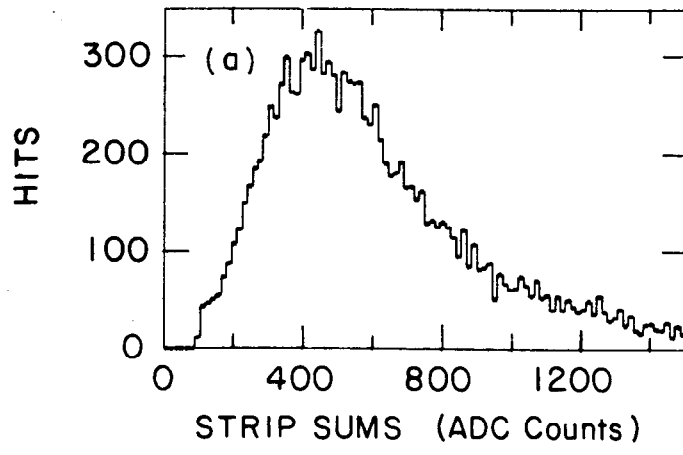
5996A7

Fig. 13



11-87
5894A4

Fig. 14



6-88
5996A16

Fig. 15

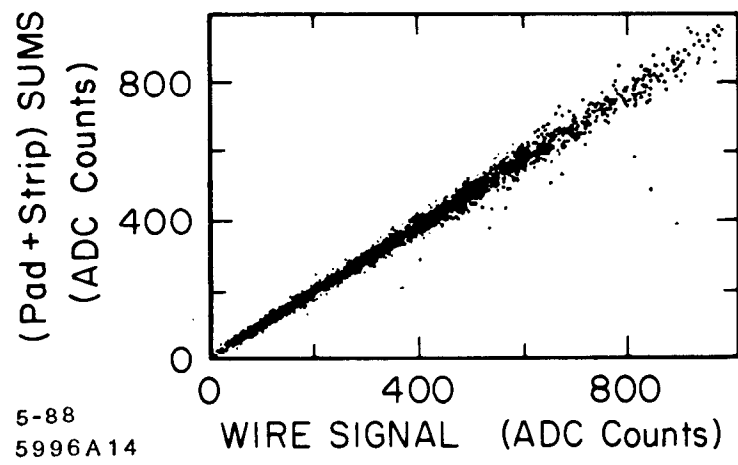


Fig. 16

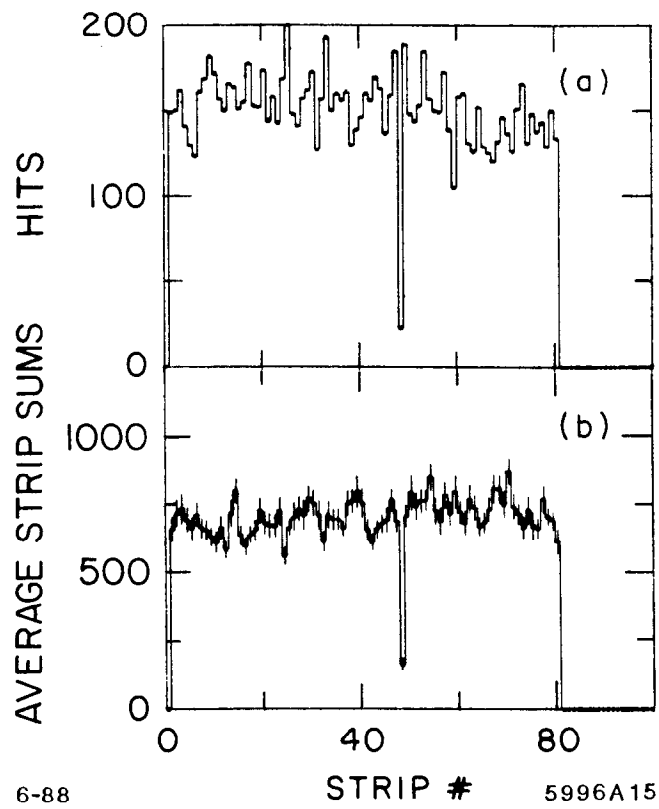


Fig. 17